Low-mass dilepton production through transport processes in a quark-gluon plasma

Yukinao Akamatsu,[1,2] Hideki Hamagaki,[3] Tetsuo Hatsuda,[2,4] and Tetsufumi Hirano[2,5]

[1]*Kobayashi-Maskawa Institute for the Origin of Particles and the Universe (KMI), Nagoya University, Nagoya 464-8602, Japan*
[2]*Department of Physics, The University of Tokyo, Tokyo 113-0033, Japan*
[3]*Center for Nuclear Study, The University of Tokyo, Tokyo 113-0033, Japan*
[4]*Theoretical Research Division, Nishina Center, RIKEN, Wako 351-0198, Japan*
[5]*Department of Physics, Sophia University, Tokyo 102-8554, Japan*

We attempt to understand the low-mass dielectron enhancement observed by the PHENIX Collaboration at the Relativistic Heavy Ion Collider by transport peak in the spectral function. On the basis of the second-order formalism of relativistic dissipative hydrodynamics, we parametrize the spectral function in low-frequency and long-wavelength regions by two transport coefficients, electric diffusion coefficient D and relaxation time τ_J, and compare our theoretical dielectron spectra with the experimental data. We study the spectrum of dielectrons produced in relativistic heavy-ion collisions by using the profile of matter evolution under full $(3 + 1)$-dimensional hydrodynamics. We find that the experimental data require the diffusion coefficient to be $D \geqslant 2/T$, with T being temperature. Our analysis shows that dielectrons emitted through the transport process mainly come from the high-temperature quark-gluon plasma phase.

PACS number(s): 25.75.Cj, 25.75.Nq, 47.75.+f

I. INTRODUCTION

Study of the quark-gluon plasma (QGP) is currently under way at the Relativistic Heavy Ion Collider (RHIC) at Brookhaven National Laboratory (BNL) and at the Large Hadron Collider (LHC) at the European Organization for Nuclear Research (CERN). At RHIC, signatures of the strongly correlated QGP have been accumulated through the analyses of the collective evolution of hot QCD matter [1–3] and of the energy loss of jets and heavy quarks [4,5]. Electromagnetic probes (i.e., photons and dileptons) are also important probes of the QCD matter since they are not contaminated by strong interaction and reflect the transport property of the matter.

Recently, the PHENIX Collaboration at RHIC reported enhancement of dielectrons in the low-mass $(0.1 < m_{ee} < 0.75$ GeV) region in Au + Au collisions [6,7].[1] However, theoretical models, which were successful in reproducing the low-mass dilepton spectra at the Super Proton Synchrotron (SPS), cannot explain the PHENIX data. This indicates the existence of yet unknown sources beyond the standard thermal radiations [9–14]. By modeling the spectral function based on the two scenarios discussed in the literature, the dropping mass and the width broadening, and combining it with the full $(3 + 1)$-dimensional hydrodynamic evolution, we also find that our model spectral function cannot explain the low-mass enhancement at PHENIX. (See Appendix A for details.) As pointed out in Ref. [11], one of the possible candidates that has a tendency to fill the gap could be the processes considered in the Landau-Pomeranchuk-Migdal resummation, such as the off-shell annihilation process $q + q + \bar{q} \rightarrow q + \gamma^* \rightarrow q + e^+ + e^-$ [15]. However, the use of perturbative picture near the transition temperature is not necessarily justified.

The main purpose of this paper is to study transport peak in the spectral function and its consequences on dilepton spectra in the low-mass region. Since the transport peak gives a divergent dielectron rate in the low-frequency limit $\omega \rightarrow 0$, this could be a possible source of the low-mass enhancement. The transport peak reflects the transport property of the QCD matter and makes the nonperturbative analyses available but has not been fully considered in the above calculations. In particular, we study the transport peak from electric charge diffusion, which reflects the diffusive motion of charged particles, that is, quarks (charged hadrons) in the QGP (hadronic) phase. Perturbative calculations of the transport coefficients and spectral function in low-frequency region [16–21] require higher-order resummation and thus the transport peak originates from various multiple scattering processes. Instead of taking the perturbative result, we parametrize the transport peak at low frequency and long wavelength by a set of transport coefficients, the electric charge diffusion coefficient D, and relaxation time τ_J [22,23]. Then we try to constrain their values by analyzing the dielectron data at PHENIX with the use of the full $(3 + 1)$-dimensional hydrodynamics simulation and the state-of-the-art lattice equation of state. Furthermore, we compare the resultant constraint with the perturbative QCD estimate at weak coupling [17–19] and the AdS/CFT estimate at strong coupling [24]. We find that the main source of the low-mass dielectrons emitted through the transport process is the high-temperature QGP, not the low-temperature hadronic phase.

In Sec. II, we review the basics of the relativistic hydrodynamic model. In Sec. III, we utilize the second-order formalism of relativistic dissipative hydrodynamics in the presence of an external electromagnetic field to obtain the spectral function parametrized with two transport coefficients, D and τ_J. Then, we calculate dielectron production using the spectral function with a transport peak and compare the results with the experimental data. In Sec. IV, we give conclusion and outlook.

---

[1]A recent measurement by the STAR Collaboration [8] is inconsistent with the PHENIX data [6,7]. We concentrate on analyzing the PHENIX data in this paper.

II. RELATIVISTIC HYDRODYNAMICS

The relativistic hydrodynamic model has been quite successful in describing collective flow phenomena in heavy-ion collisions at RHIC [1–3]. Its basic equation for perfect fluids reads

$$\partial_\mu T^{\mu\nu} = 0, \quad T^{\mu\nu} = (e + P)u^\mu u^\nu - Pg^{\mu\nu}, \tag{1}$$

where $T^{\mu\nu}$ is the energy-momentum tensor, e is the energy density, P is the pressure, and u^μ is the fluid velocity. The baryon chemical potential is neglected, since it is small near midrapidity at RHIC and LHC energies.

A. Lattice equation of state and spacetime evolution

The energy density and pressure are related through the equation of state (EoS) $P = P(e)$. In the present paper, we use one of the latest EoSs obtained from $(2 + 1)$-flavor lattice

QCD simulations with a Symanzik improved gauge action and a stout-link improved staggered fermion action [25]. The parametrization of the trace anomaly $I \equiv e - 3P$ given in [25] reads

$$\frac{I(T)}{T^4} = \exp(-h_1/t - h_2/t^2)\left(h_0 + \frac{f_0[\tanh(f_1 t + f_2) + 1]}{1 + g_1 t + g_2 t^2}\right), \tag{2}$$

where $t \equiv T/(0.2 \text{ GeV})$, $(h_0, h_1, h_2) = (0.1396, -0.1800, 0.0350)$, $(f_0, f_1, f_2) = (2.76, 6.79, -5.29)$, and $(g_1, g_2) = (-0.47, 1.04)$. As shown in Fig. 1, the lattice EoS shows a smooth crossover from the hadronic phase to the QGP phase in contrast to the historic bag EoS, which has the first-order phase transition.

In solving hydrodynamic equation Eq. (1), we pose the initial condition at $\tau_0 = 0.6$ fm/c for entropy density s and flow vector $\vec{u}$:

$$\tau_0 s(\eta_s, \vec{x}_\perp) = C\theta(y_b - |\eta_s|)f^{pp}(\eta_s)\left[a\left(\frac{y_b - \eta_s}{y_b}\frac{dN_{part}^A}{d^2 x_\perp} + \frac{y_b + \eta_s}{y_b}\frac{dN_{part}^B}{d^2 x_\perp}\right) + (1 - a)\frac{dN_{coll}}{d^2 x_\perp}\right], \tag{3}$$

$$u_z = \sinh \eta_s, \quad u_x = u_y = 0, \tag{4}$$

when nucleus A (B) is traveling along the z-axis in the negative (positive) direction. Here y_b (>0) is the beam rapidity, $C = 13.0$ and $a = 0.85$ are fitting parameters, $dN_{part}^{A(B)}/d^2 x_\perp$, $dN_{coll}/d^2 x_\perp$ are defined in the Glauber model [26], and $f^{pp}(\eta_s)$ is a parametrization of the shape of rapidity distribution in proton-proton ($p + p$) collision at $\sqrt{s_{NN}} = 200$ GeV. For details of the initial condition, see Refs. [27–30]. With this initial condition, hydrodynamic equations Eq. (1) are numerically solved assuming chemical equilibrium above freezeout temperature T_f, which we determine as follows.

At $T = T_f$, the Cooper-Frye formula [31] converts the profile of hydrodynamic evolution $(\vec{u}, T)$ into spectra of
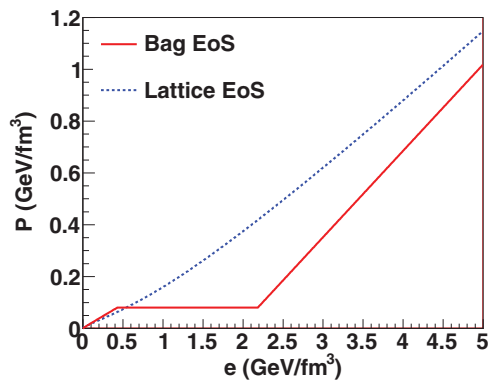

FIG. 1. (Color online) Pressure as a function of energy density $P = P(e)$ compared with the conventional bag equation of state and the lattice equation of state [25]. In the bag model at $T = 170$ MeV, pressure with $N_f = 3$ massless free ideal QGP gas is matched to that of a hadron resonance gas including resonances up to $\Delta(1232)$. The resultant bag constant is $B^{1/4} = 247$ MeV.

particles and resonances [up to $\Delta(1232)$] by

$$E\frac{dN_i}{d^3 p} = \frac{d_i}{(2\pi)^3}\int_{\partial\Sigma}\frac{p^\mu d\sigma_\mu}{\exp[p^\mu u_\mu/T_f] \mp 1}, \tag{5}$$

where d_i is the degeneracy factor of hadron species i, the sign in the denominator is $-$ (+) for bosons (fermions), $\partial\Sigma$ is the spacetime hypersurface satisfying $T(\tau, \eta_s, x, y) = T_f$, and $d\sigma^\mu$ is its element. To obtain the spectra of stable particles, the decay products from $\Delta(1232)$ are also included. We determine the thermal freezeout temperature T_f by fitting the experimental slope of the proton p_T spectra as shown in Fig. 2. The slopes can be fitted well by $T_f = 0.15$ GeV. The impact parameters of the simulation are $b = 7.1$ fm (20–30% centrality) and $b = 9.7$ fm (40–50% centrality). Note that we have multiplied a factor ≈ 1.4 to fit the absolute magnitude of the experimental data at $p_T = 1.0$ GeV. This slight difference in the magnitude between hydrodynamical calculation and experimental data is possibly due to an absence of chemical freezeout mechanism [28] in the lattice equation of state.

B. Dielectron spectrum

Here we briefly summarize the formula for the dielectron production from an expanding medium in relativistic heavy-ion collisions. Since the invariant mass of our interest is $\sqrt{q^2} \geqslant 0.1$ GeV, we neglect the electron mass in the following. The $(3 + 1)$-dimensional hydrodynamic model gives each spacetime point a local flow vector $u^\mu(x)$ and a local temperature $T(x)$. Each spacetime volume under hydrodynamic
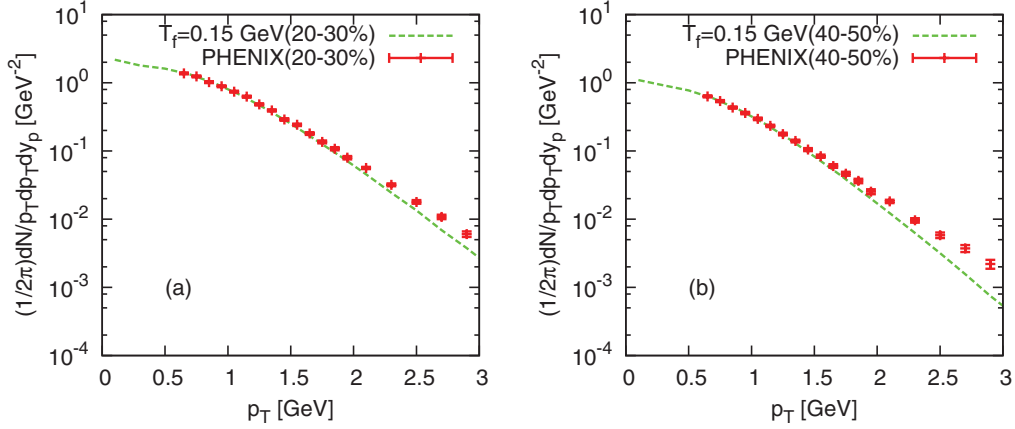
FIG. 2. (Color online) Shown is the hydrodynamic calculation for the slope of $p_{\rm T}$ spectra of protons with freezeout temperature $T_{\rm f} = 0.15$ GeV. The $p_{\rm T}$ spectra are calculated by the hydrodynamic model with lattice EoS. In the hydrodynamic calculation, chemical equilibrium is assumed at $T > T_{\rm f} = 0.15$ GeV. The impact parameters of the collision are (a) $b = 7.1$ fm (20–30% centrality) and (b) $b = 9.7$ fm (40–50% centrality) in the hydrodynamic calculation. Note that overall $p_{\rm T}$ spectra are scaled (by multiplying ≈ 1.4) to match the experimental data at $p_{\rm T} = 1.0$ GeV.

evolution emits lepton pairs with the rate [32,33]

$$\frac{E_1 E_2 dN}{d^3 p_1 d^3 p_2 d^4 x} = \frac{\alpha^2}{2\pi^4 q^4} \frac{p_1^\mu p_2^\nu + p_2^\mu p_1^\nu - \frac{q^2}{2} g^{\mu\nu}}{\exp(q^0/T) - 1} \times \mathrm{Im} G_{{\rm R},\mu\nu}(q; T), \tag{6}$$

$$G_{\rm R}^{\mu\nu}(q; T) \equiv \int d^4 x e^{iqx} i\theta(x^0) \langle [J^\mu(x), J^\nu(0)] \rangle_T, \tag{7}$$

$$J^\mu(x) \equiv \frac{2}{3} \bar{\rm u} \gamma^\mu {\rm u} - \frac{1}{3} \bar{\rm d} \gamma^\mu {\rm d} - \frac{1}{3} \bar{\rm s} \gamma^\mu {\rm s} \tag{8}$$

when observed in the local fluid rest frame. In the laboratory frame, momentum distribution of the lepton pairs emitted from the thermal medium in heavy-ion collisions is expressed by the following integration:

$$\frac{E_1 E_2 dN}{d^3 p_1 d^3 p_2} = \int_\Sigma d^4 x \frac{\alpha^2}{2\pi^4 \tilde{q}^4} \frac{\tilde{p}_1^\mu \tilde{p}_2^\nu + \tilde{p}_2^\mu \tilde{p}_1^\nu - \frac{\tilde{q}^2}{2} g^{\mu\nu}}{\exp[\tilde{q}^0/T(x)] - 1} \times \mathrm{Im} \tilde{G}_{{\rm R},\mu\nu}(\tilde{q}; T(x)). \tag{9}$$

Σ indicates the spacetime region of the hot QCD medium with $T > T_{\rm f}$, which is considered to radiate dielectrons. The $\tilde{A}^{\mu\nu\cdots}$ denotes a Lorentz tensor in the local rest frame boosted by u^μ from that in the laboratory frame $A^{\mu\nu\cdots}$.

In the PHENIX experiment, with which we will compare our results later, the acceptance of each electron or positron depends on the detector geometry and on the particle kinematics [6,7]. We introduce an acceptance function $A(p_1, p_2)$ to pick up the phase space where both the electron and positron are in the acceptance. The dielectron invariant mass spectrum from the expanding medium is therefore given by

$$\frac{dN}{dm_{ee}} = 2m_{ee} \int d^3 p_1 d^3 p_2 \frac{dN}{d^3 p_1 d^3 p_2} A(p_1, p_2) \delta(q^2 - m_{ee}^2). \tag{10}$$

III. MODEL OF LOW-MASS DILEPTONS: TRANSPORT PEAK

One of the promising nonperturbative approaches to explain the low-mass enhancement is to utilize the transport theory, which parameterizes the spectral function in low-energy and long-wavelength region with transport coefficients. The transport process we consider is the electric charge diffusion of quarks (charged hadrons) in the QGP (hadron) phase.

A. Linearized hydrodynamics with external field

Here we construct retarded correlator $G_{\rm R}^{\mu\nu}(q; T)$ and corresponding spectral function (transport-SPF) from the linear analysis of transport equations. According to the linear response theory, the retarded correlator relates small perturbation $\delta H(t) = \int d^3 x J^\mu(x) \delta A_\mu(x)$ and system response $\langle \delta J^\mu(q) \rangle_T$ in the linear order [22]:

$$\langle \delta J^\mu(q) \rangle_T = -G_{\rm R}^{\mu\nu}(q; T) \delta A_\nu(q), \tag{11}$$

where $f(q) \equiv \int d^4 x e^{iqx} f(x)$. Hereafter we calculate the linear relation between δJ^μ and δA_ν on the basis of relativistic dissipative hydrodynamics.

In the presence of external field δA^μ, conservation laws for the energy-momentum tensor $T^{\mu\nu}$ and the electric current J^μ are modified to

$$\partial_\nu T^{\nu\mu} = F^{\mu\nu} J_\nu, \tag{12}$$

$$\partial_\mu J^\mu = 0, \tag{13}$$

where we define $F_{\mu\nu} \equiv \partial_\mu \delta A_\nu - \partial_\nu \delta A_\mu$, $\vec{E} \equiv -\vec{\nabla}\delta A^0 - \frac{\partial \delta \vec{A}}{\partial t}$, and $\vec{B} \equiv \vec{\nabla} \times \delta \vec{A}$. In relativistic viscous hydrodynamics in

Landau frame [34],[2] the energy-momentum tensor $T^{\mu\nu}$ and the electric current J^μ are decomposed as

$$T^{\mu\nu} = eu^\mu u^\nu - (P + \Pi)\triangle^{\mu\nu} + \pi^{\mu\nu}, \qquad (14)$$

$$J^\mu = \rho u^\mu + \nu^\mu, \qquad (15)$$

$$\triangle^{\mu\nu} \equiv g^{\mu\nu} - u^\mu u^\nu, \qquad (16)$$

with bulk pressure Π, shear stress tensor $\pi^{\mu\nu}$, and dissipative electric current ν^μ satisfying $\pi^{\mu\nu}u_\nu = 0$, $\pi^\mu_\mu = 0$, $\nu^\mu u_\mu = 0$. The scalar quantities e, P, and ρ satisfy the equation of state $P = P(e, \rho)$ derived in equilibrium. The entropy current in the second-order formalism constructed by Israel and Stewart [35,36] is decomposed as

$$s^\mu = su^\mu - \frac{\mu}{T}\nu^\mu - \frac{1}{T}(\alpha_0 \Pi \nu^\mu + \alpha_1 \pi^{\mu\nu}\nu_\nu)$$
$$- \frac{u^\mu}{2T}(\beta_0 \Pi^2 - \beta_1 \nu^\mu \nu_\mu + \beta_2 \pi^{\rho\sigma}\pi_{\rho\sigma}), \qquad (17)$$

with positive transport coefficients α_a ($a = 0, 1$) and β_b ($b = 0, 1, 2$) and chemical potential μ for the electric charge. Here s is the entropy density $s(e, \rho)$ derived from the equation of state. Calculating the divergence of the entropy current up to quadratic order in Π, $\pi^{\mu\nu}$, ν^μ, and $F^{\mu\nu}$ and in derivatives of e, ρ, and u^μ, we obtain

$$\partial_\mu s^\mu = -\frac{\Pi}{T}(\partial_\mu u^\mu + \alpha_0 \partial_\mu \nu^\mu + \beta_0 \dot{\Pi})$$
$$+ \frac{\pi^{\mu\nu}}{T}(\partial_\mu u_\nu - \alpha_1 \partial_\mu \nu_\nu - \beta_2 \dot{\pi}_{\mu\nu}) - \frac{\nu^\mu}{T}\left[T\partial_\mu\left(\frac{\mu}{T}\right)\right.$$
$$\left. + F_{\mu\nu}u^\nu + \alpha_0 \partial_\mu \Pi + \alpha_1 \partial_\nu \pi^\nu_\mu - \beta_1 \dot{\nu}_\mu \right], \qquad (18)$$

where $\dot{f} \equiv u^\mu \partial_\mu f$. The second law of thermodynamics requires the following constitutive equations:

$$-\Pi = \zeta(\partial_\mu u^\mu + \alpha_0 \partial_\mu \nu^\mu + \beta_0 \dot{\Pi}), \qquad (19)$$

$$\pi_{\mu\nu} = 2\eta\langle\langle(\partial_\mu u_\nu - \alpha_1 \partial_\mu \nu_\nu - \beta_2 \dot{\pi}_{\mu\nu})\rangle\rangle, \qquad (20)$$

$$\nu^\mu = \sigma \triangle^{\mu\rho}\left[T\partial_\rho\left(\frac{\mu}{T}\right) + F_{\rho\sigma}u^\sigma + \alpha_0 \partial_\rho \Pi\right.$$
$$\left. + \alpha_1 \partial_\sigma \pi^\sigma_\rho - \beta_1 \dot{\nu}_\rho \right], \qquad (21)$$

with bulk and shear viscosities ζ, η (≥ 0), and electrical conductivity σ (≥ 0). Here $\langle\langle B^{\mu\nu}\rangle\rangle$ stands for a spatial, symmetric, and traceless tensor extracted from a general tensor $B^{\mu\nu}$:

$$\langle\langle B^{\mu\nu}\rangle\rangle \equiv \triangle^{\mu\rho}\triangle^{\nu\sigma}\left[\frac{B_{\rho\sigma} + B_{\sigma\rho}}{2} - \frac{\triangle_{\rho\sigma}\triangle^{\alpha\beta}B_{\alpha\beta}}{3}\right]. \qquad (22)$$

---

[2]Since we are interested in the quark-gluon plasma at vanishing chemical potential, the Eckart frame, in which we define the flow vector by u^μ by $J^\mu = \rho u^\mu$, is inconvenient. This is because the electric current is $J^\mu = (0, 0, 0, 0)$ in equilibrium and hence u^μ becomes ill defined.

When the system is close to equilibrium, the energy density $e(x)$, the charge density $\rho(x)$, and the flow vector $u^\mu(x)$ slightly deviate from their equilibrium quantities:

$$e(x) = e + \delta e(x), \qquad (23)$$

$$\rho(x) = \rho + \delta\rho(x), \qquad (24)$$

$$u^\mu(x) = (1, \ \delta\vec{u}(x)). \qquad (25)$$

Neglecting for simplicity the couplings $\alpha_{0,1}$ between different dissipative modes, the dissipative part of the electric current $\nu^\mu(x)$ is then given by

$$\nu^0(x) = 0, \qquad (26)$$

$$\vec{v}(x) = -\sigma\left[T\vec{\nabla}\left(\frac{\mu}{T}\right) - \vec{E} + \beta_1 \partial_t \vec{v}\right], \qquad (27)$$

in the linear order in δe, $\delta\rho$, $\delta\vec{u}$, and A^μ. Explicitly in terms of δe and $\delta\rho$,

$$T\vec{\nabla}\left(\frac{\mu}{T}\right) = \frac{1}{X}\left(\frac{\partial e}{\partial T} + \frac{\mu}{T}\frac{\partial e}{\partial \mu}\right)\vec{\nabla}\delta\rho$$
$$- \frac{1}{X}\left(\frac{\partial\rho}{\partial T} + \frac{\mu}{T}\frac{\partial\rho}{\partial\mu}\right)\vec{\nabla}\delta e, \qquad (28)$$

$$X \equiv \frac{\partial e}{\partial T}\frac{\partial\rho}{\partial\mu} - \frac{\partial e}{\partial\mu}\frac{\partial\rho}{\partial T}. \qquad (29)$$

In the quark-gluon plasma with vanishing baryon density, $\rho = 0$, we have $\frac{\partial e}{\partial\mu} = 0$ and $\frac{\partial\rho}{\partial T} = 0$, so that the electric current is obtained as

$$J^\mu(x) = (\delta\rho(x), \vec{v}(x)), \qquad (30)$$

$$\vec{v}(x) = \sigma\vec{E} - D\vec{\nabla}\delta\rho - \tau_J\frac{\partial\vec{v}}{\partial t}, \qquad (31)$$

$$D = \frac{\sigma}{\chi}, \quad \tau_J = \beta_1\sigma, \quad \chi = \frac{\partial\rho}{\partial\mu}. \qquad (32)$$

The dynamics of the electric current $J^\mu(x)$ is obtained in a closed form, while with finite electric charge density there arises a coupling between the sound mode $\delta e(x)$ and the dissipative electric current $\nu^\mu(x)$ even after ignoring $\alpha_{0,1}$. This is because energy current, or momentum, carries electric charge at finite density $\mu \neq 0$.

Combining Eqs. (13), (15), and (31), we obtain

$$J^0(q) = \frac{\sigma[-k^2\delta A_0(q) - \omega k^i\delta A_i(q)]}{-\tau_J\omega^2 - i\omega + Dk^2}, \qquad (33)$$

$$J^i(q) = \frac{-\sigma\omega k^i}{-\tau_J\omega^2 - i\omega + Dk^2}\left(\delta A_0(q) + \frac{\omega k^j\delta A_j(q)}{k^2}\right)$$
$$+ \frac{\sigma\omega}{-\tau_J\omega - i}\left(-\delta A_i(q) + \frac{k^i k^j\delta A_j(q)}{k^2}\right), \qquad (34)$$

where $q^\mu = (\omega, \vec{k})$ and upper and lower Lorentz indices matter, $k_x = k^{i=1} = -k_{i=1}$ for example. The retarded correlators are given by

$$G_R^{00}(\omega, \vec{k}; T) = \frac{\sigma k^2}{-\tau_J\omega^2 - i\omega + Dk^2}, \qquad (35)$$

$$G_R^{0i}(\omega, \vec{k}; T) = G_R^{i0}(\omega, \vec{k}; T) = \frac{\sigma\omega k^i}{-\tau_J\omega^2 - i\omega + Dk^2}, \qquad (36)$$

$$G_R^{ij}(\omega, \vec{k}; T) = \frac{\sigma\omega}{-\tau_J\omega - i}\left(\delta^{ij} - \frac{k^i k^j}{k^2}\right)$$
$$+ \frac{\sigma\omega^2}{-\tau_J\omega^2 - i\omega + Dk^2}\frac{k^i k^j}{k^2}, \quad (37)$$

which are decomposed into two independent parts, namely longitudinal and transverse parts:

$$G_R^{(L)}(\omega, \vec{k}; T) \equiv -\frac{q^2}{k^2}G_R^{00}(\omega, \vec{k}; T) = \frac{\sigma q^2}{\tau_J\omega^2 - Dk^2 + i\omega}, \quad (38)$$

$$G_R^{(T)}(\omega, \vec{k}; T) \equiv \frac{1}{2}(G_{R,\mu}^{\mu}(\omega, \vec{k}; T) - G_R^{(L)}(\omega, \vec{k}; T))$$
$$= \frac{\sigma\omega}{\tau_J\omega + i}. \quad (39)$$

Note that the poles of Eqs. (38) and (39) are always located in the lower half of the ω plane. Corresponding two independent components of the spectral function are

$$\mathrm{Im}G_R^{(L)}(\omega, \vec{k}; T) = -\frac{\sigma\omega q^2}{\omega^2 + (\tau_J\omega^2 - Dk^2)^2}, \quad (40)$$

$$\mathrm{Im}G_R^{(T)}(\omega, \vec{k}; T) = -\frac{\sigma\omega}{\tau_J^2\omega^2 + 1}, \quad (41)$$

with $\mathrm{Im}G_{R,\mu}^{\mu} = 2\mathrm{Im}G_R^{(T)} + \mathrm{Im}G_R^{(L)}$.

Due to the analyticity of $G_R^{(L,T)}(\omega, \vec{k}; T)$ in the upper half of the ω plane, the following one-subtracted Kramers-Kronig relation is satisfied by Eqs. (38) and (39) *irrespective* of the values of σ, D, and τ_J:

$$\mathrm{Re}\big[G_R^{(L,T)}(\omega, \vec{k}; T)\big] - \frac{\sigma}{\tau_J} = \int_{-\infty}^{\infty}\frac{d\omega'}{\pi}P\left(\frac{1}{\omega' - \omega}\right)$$
$$\times \mathrm{Im}\big[G_R^{(L,T)}(\omega', \vec{k}; T)\big]. \quad (42)$$

As a consistency check, let us consider the charge fluctuation $\chi \equiv \mathrm{Re}[G_R^{(L)}(\omega = 0, \vec{k} \to \vec{0}; T)] = \frac{\sigma}{\tau_J} + \int_{-\infty}^{\infty}\frac{d\omega'}{\pi}\frac{\mathrm{Im}[G_R^{(L)}(\omega', \vec{k} \to \vec{0}; T)]}{\omega'}$. By using the information of $\mathrm{Im}[G_R^{(L)}]$ obtained from Eq. (40) in the timelike ($\omega \geqslant |\vec{k}|$) and the spacelike ($\omega < |\vec{k}|$) regions, one finds $\chi = \sigma/D$, which is nothing but the relation in Eq. (32) obtained from the linearized hydrodynamics under an external field.

To illustrate the effect of D, τ_J, and σ to the dilepton emission rate, let us now consider the scaled spectral function $\Sigma(q; T) \equiv -\mathrm{Im}G_{R,\mu}^{\mu}(q; T)/(3q^2) = -[\frac{2}{3}\mathrm{Im}G_R^{(T)} + \frac{1}{3}\mathrm{Im}G_R^{(L)}]/q^2$. Since the timelike kinematics, $\omega \geqslant |\vec{k}|$, is relevant for dileptons, let us consider an extreme case,

$$\Sigma(\omega \neq 0, |\vec{k}| = 0; T) = \frac{1}{\omega}\frac{\sigma}{\tau_J^2\omega^2 + 1}, \quad (43)$$

where the transverse component and the logitidinal component contribute with 2 to 1 ratio. (In our numerical calculation later, we use the spectral function with full ω and $\vec{k}$ dependence.) Equation (43) indicates a large enhancement of the dilepton emmission rate near $\omega = 0$ with a typical width τ_J^{-1} (Fig. 3). Also, the rate becomes large for large conductivity and/or small relaxation time.
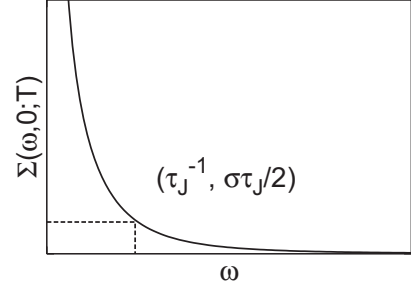

FIG. 3. Scaled transport-spectral function (SPF) $\Sigma(\omega, \vec{0}; T)$. It diverges as $\Sigma \propto 1/\omega$ in the limit $\omega \to 0$.

Although we have demonstrated the derivation in a one-flavor case, generalization to the multiflavor case is straightforward. We discuss in Appendix B that the transport equation Eq. (31) holds in the three-flavor case under three assumptions: (i) There is no coupling between the dissipative modes in the decomposition of the entropy current. (ii) Transport coefficients are flavor-independent. (iii) Quark number susceptibility matrix is proportional to the unit matrix $\chi_{ij} \propto \delta_{ij}$. Here $\chi_{ij} \equiv \frac{\partial n_i}{\partial\mu_j}$ and n_i (μ_i) is a quark number density (quark number chemical potential) for a flavor i. $\chi_{ij} \equiv \frac{\partial n_i}{\partial\mu_j}$ is measured by a lattice QCD simulation [37] and is found to satisfy $\chi_{ij} \propto \delta_{ij}$ approximately.

B. Diffusion coefficient and relaxation time

In the following, we use (D, τ_J, χ) instead of (D, τ_J, σ) as independent parameters to parametrize the spectral function. The electric charge susceptibility χ can be expressed in terms of the quark number susceptibility by

$$\chi = \frac{4}{9}\chi_{uu} + \frac{1}{9}\chi_{dd} + \frac{1}{9}\chi_{ss} - \frac{4}{9}\chi_{ud} - \frac{4}{9}\chi_{us} + \frac{2}{9}\chi_{ds} \approx \frac{2}{3}\chi_{uu}, \quad (44)$$

which can be fitted to the result of lattice QCD simulation [37] as follows:

$$\chi(T, \mu = 0) \approx 0.28T^2\left[1 + \tanh\left(\frac{T - T_c^*}{0.15T_c^*}\right)\right]. \quad (45)$$

We take T_c^* to be the temperature at the center of the chiral crossover transition $T_c^* \approx 0.155$ GeV (see Fig. 4 (right) in [38]). We parametrize D and τ_J as

$$D \propto \frac{1}{T}, \quad \tau_J \propto \frac{1}{T}, \quad (46)$$

for dimensional reasons.[3] To see the typical magnitude of the transport coefficients of weakly and strongly coupled plasmas, we refer to the results obtained by perturbative QCD [17–19]

---

[3]We can also parametrize $\tau_J \propto 1/T$ and $\sigma \propto T$ assuming the scaling to temperature. This parametrization differs from the one adopted in our study only below the transition region $T < T_c^*$ if we fix the higher temperature ($T \sim 2T_c^*$) behavior.
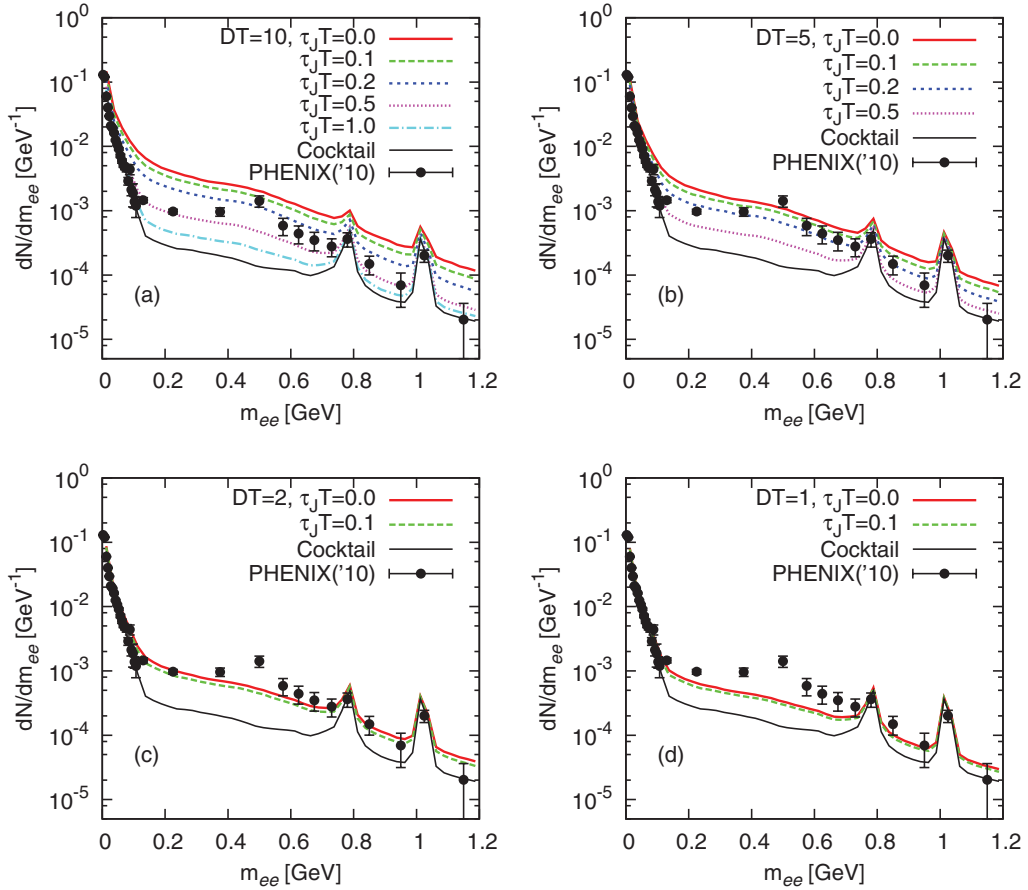
FIG. 4. (Color online) We compare in (a)–(d) the dielectron spectrum dN/dm_{ee} calculated with the transport-SPF and the corresponding experimental data [7]. In the transport-SPF, diffusion coefficient is fixed to D values of (a) $10/T$, (b) $5/T$, (c) $2/T$, and (d) $1/T$. The relaxation time τ_J is varied in $(0.0–1.0)/T$. We take into account the contributions from the hadronic decays after freezeout (denoted as "Cocktail" in these figures). We plot only the statistical errors for experimental data.

with $g \approx 2$,

$$D^{\text{pQCD}} \approx D_q^{\text{pQCD}} \approx \frac{0.150}{\alpha_s^2 \ln(0.461/\alpha_s)T} \approx \frac{4}{T}, \quad (47)$$

$$\tau_J^{\text{pQCD}} \approx 3.748 \times D^{\text{pQCD}} \approx \frac{15}{T}, \quad (48)$$

and those by AdS/CFT [24],

$$D^{\text{AdS/CFT}} = \frac{1}{2\pi T}, \quad \tau_J^{\text{AdS/CFT}} = \frac{\ln 2}{2\pi T}. \quad (49)$$

Here D_q^{pQCD} stands for *quark number* diffusion coefficient. We can show $D = D_q$ within the same approximation as used in the derivation of the constitutive equation in the multiflavor case. (See Appendix B.)

C. Comparison to experimental data

We calculate the theoretical spectrum of dilepton production using Eq. (10). Note that, on the one hand, our spectral function is calculated by the transport theory and contains dynamical information of QCD matter close to equilibrium. On the other hand, the equation of state used in the hydrodynamic calculation is the one in equilibrium in all the temperature

above T_f. The minimum bias theoretical spectrum is calculated by

$$\frac{dN^{\text{min.bias}}}{dm_{ee}} = \frac{1}{10} \times \left[\frac{dN^{0-10\%}}{dm_{ee}} + \cdots + \frac{dN^{90-100\%}}{dm_{ee}} \right]$$

$$\approx \frac{1}{10} \times \left[\frac{dN^{0-10\%}}{dm_{ee}} + \cdots + \frac{dN^{50-60\%}}{dm_{ee}} \right], \quad (50)$$

neglecting peripheral collisions with centrality 60–100% because their contributions are small.

In Figs. 4(a)–4(d), we compare the dielectron spectrum dN/dm_{ee} calculated with the transport-SPF with the experimental data. The dilepton from the transport process is dominant around $m_{ee} \sim 0.5$ GeV due to the $1/\omega$ long tail, and the dilepton from Dalitz decay becomes important only for $m_{ee} < 0.1$ GeV. The parametrization for the diffusion coefficient is (a) $D = 10/T$, (b) $D = 5/T$, (c) $D = 2/T$, and (d) $D = 1/T$ and that for the relaxation time is varied in $\tau_J = (0.0–1.0)/T$. We add the dielectrons from hadronic decays after freezeout (hadronic cocktail) [7] to the thermal contribution from the transport-SPF. We find that our results with $(DT, \tau_J T) = (10, 0.5)$, $(5, 0.2)$, and $(2, 0.0–0.1)$ give dielectron spectra comparable to the experimental data. These values are rather different from the theoretical estimates,
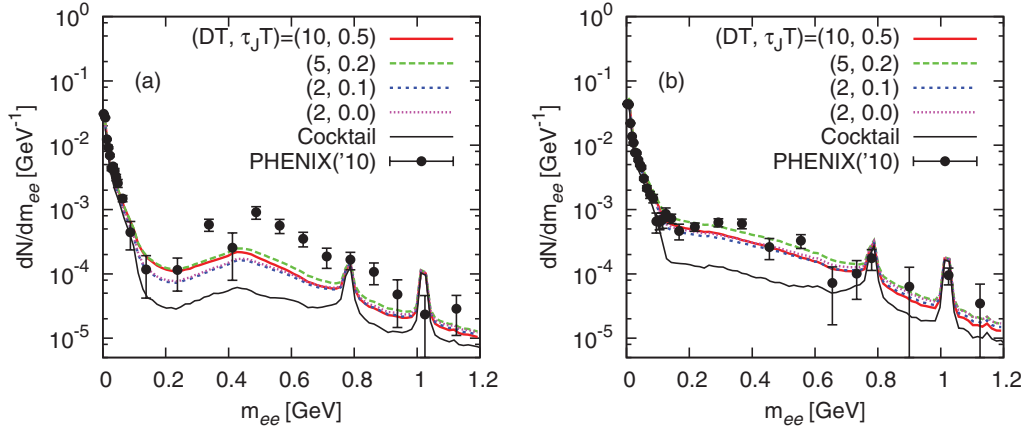
FIG. 5. (Color online) In panels (a) and (b), we compare our calculation of the dielectron spectrum with restricted p_T windows and the experimental data [7]. The dielectron spectrum dN/dm_{ee} is restricted in (a) $0.0 < p_T < 0.5$ GeV and (b) $0.5 < p_T < 1.0$ GeV. We calculate with parameter sets $(DT, \tau_J T) = (10, 0.5)$, $(5, 0.2)$, and $(2, 0.0\text{–}0.1)$ in the transport-SPF. The hadronic decays after freezeout are taken into account (denoted as "Cocktail" in these figures). In panels (a) and (b), we only plot the statistical errors for experimental data.

$(D^{pQCD}T, \tau_J^{pQCD}T) \approx (4, 15)$ and $(D^{AdS/CFT}T, \tau_J^{AdS/CFT}T) = (\frac{1}{2\pi}, \frac{\ln 2}{2\pi})$. From (c) and (d), we also find that experimental data set a lower bound for the diffusion coefficient $D \geqslant 2/T$ because the dielectron rate is largest with $\tau_J = 0$ for fixed D.

Next we study the dielectron spectrum in more detail. In Figs. 5(a) and 5(b), we show the dielectron invariant mass spectrum with the dielectron transverse momentum restricted in (a) $0 \leqslant p_T \leqslant 0.5$ GeV and (b) $0.5 \leqslant p_T \leqslant 1.0$ GeV. We calculate these spectra with parameter sets $(DT, \tau_J T) = (10, 0.5)$, $(5, 0.2)$, and $(2, 0.0\text{–}0.1)$ in the transport-SPF. Clearly all of our calculations for low p_T window (a) undershoot the experimental data in $0.3 < m_{ee} < 0.7$ GeV, while for high p_T window (b) they all show good agreement with the data.

In Fig. 6, we show the dielectron transverse mass (m_T) distribution at midrapidity $y_p = 0$. The calculation is performed with $(DT, \tau_J T) = (10, 0.5)$, $(5, 0.2)$, and $(2, 0.0\text{–}0.1)$. We first calculate the dielectron p_T spectrum by integrating in the invariant mass range $0.3 \leqslant m_{ee} \leqslant 0.75$ GeV for each centrality. We then divide the dielectron p_T spectra by half of the number of participant nucleons ($N_{part}/2$) for each centrality. We take the horizontal axis to be $m_T - m_0 = \sqrt{p_T^2 + m_0^2} - m_0$ to obtain m_T spectra. Here m_0 is the mean value of the dielectron invariant mass with minimum bias $m_0 \equiv \langle m_{ee} \rangle$ in $0.3 \leqslant m_{ee} \leqslant 0.75$ GeV, which turns out to be $m_0 \approx 0.47$ GeV in our calculation. Experimental data are also obtained by the same procedure after subtracting other sources such as hadron decays and correcting PHENIX acceptance. The experimental data exceed the theoretical spectra at $m_T - m_0 < 0.3$ GeV while the former are comparable with the latter at $m_T - m_0 > 0.3$ GeV. This is consistent with what we found in Fig. 5.
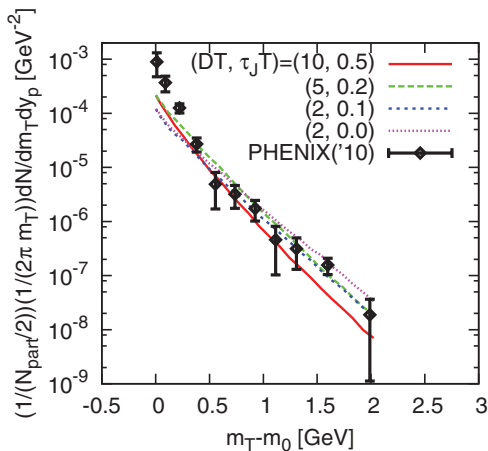

FIG. 6. (Color online) We compare the transverse mass spectrum calculated with the transport-SPF and the corresponding experimental data [7]. The parameter sets $(DT, \tau_J T)$ are the same with those in Fig. 5 In the experimental data, other sources such as hadron decays are subtracted and PHENIX acceptance is corrected. We plot only the statistical errors for experimental data.
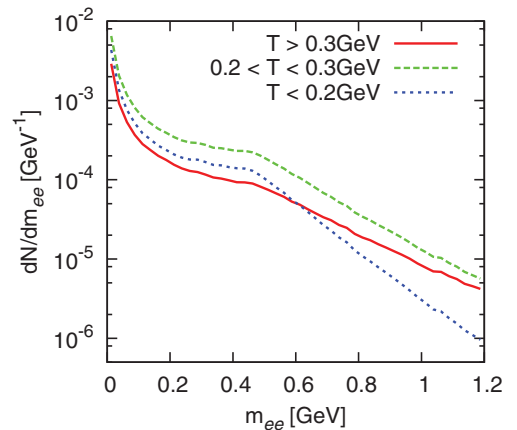

FIG. 7. (Color online) Plotted is dielectron production from the matter with $T > 0.3$ GeV, $0.2 < T < 0.3$ GeV, and $T < 0.2$ GeV. The parameter for transport-SPF is $(DT, \tau_J T) = (10, 0.5)$. The PHENIX acceptance is taken into account.

In Fig. 7, we show dielectron production from the hot matter with different temperature ranges: $T > 0.3$ GeV, $0.2 < T < 0.3$ GeV, and $T < 0.2$ GeV. Clearly the intermediate-temperature QGP phase with $0.2 < T < 0.3$ GeV is the main source for the dielectron production in spite of its small spacetime volume. This makes a sharp contrast with the expectation that the low-mass dielectrons are radiated from the low-temperature hadronic phase due to the larger spacetime volume [9]. Furthermore, this tendency may be consistent with the previous analyses at SPS, where the transport peak does not play an important role.

IV. CONCLUSION AND OUTLOOK

In this paper, we have studied the dilepton production from the hot dynamical medium in relativistic heavy-ion collisions. In particular, we have explored the relation between the low-mass dielectron enhancement and the transport property of the hot QCD matter, namely the electric charge diffusion process of quarks (hadrons) in the QGP (hadronic) phase. Because the dielectron rate from the transport-SPF is divergent at $\omega \sim 0$, it is reasonable to expect that the transport property is relevant to the low-mass dielectron enhancement. Also the transport theoretical approach enables us to treat the problem nonperturbatively.

We have conducted our analysis in the following way. We start from the second-order formalism of relativistic dissipative hydrodynamics, which introduces diffusion coefficient D and relaxation time τ_J. By performing linear analysis, we parameterized the low-frequency and long-wavelength region of the spectral function with these transport coefficients. We calculated the dielectron yield by combining the transport-SPF and the full $(3 + 1)$-dimensional hydrodynamic medium evolution with the lattice EoS and attempted to extract the transport coefficients from the data. We summarize our results in Fig. 8. We found that transport peak with parameter sets $(DT, \tau_J T) = (10, 0.5), (5, 0.2), (2, 0.0\text{–}0.1)$ can reproduce the experimental data dN/dm_{ee}. We also showed that in order to explain the data, the diffusion coefficient must be $D \geqslant 2/T$. These obtained parameter sets are rather different from both weak-coupling pQCD calculation and strong-coupling calculation on the basis of the AdS/CFT correspondence. Since there is no *a priori* relation between the transport coefficients D, τ_J and the shear viscosity η, the dilepton spectrum and elliptic flow give us useful independent information on the different aspects of the QGP. On the other hand, the large ratio $D/\tau_J \sim 20$ obtained in our analysis, which neither weak-coupling nor strong-coupling calculations predict, might indicate that the transport peak does not explain all of the dilepton enhancement observed at PHENIX. Furthermore, while these parameter sets could reproduce the more detailed experimental data dN/dm_{ee} restricted in $0.5 < p_T < 1.0$ GeV and $(1/2\pi m_T) dN/dm_T dy_p$ in $m_T - m_0 > 0.3$ GeV, they could not reproduce those restricted in $0.0 < p_T < 0.5$ GeV and in $m_T - m_0 < 0.3$ GeV. In view of these calculations, we conclude that the low-mass dielectrons at RHIC have not been fully understood theoretically despite the fact that the transport peak of the spectral function has a tendency to enhance low-mass dileptons.

Meanwhile we also found that a large portion of the thermal dielectron radiation comes from the high-temperature QGP phase with $T > 0.2$ GeV because the fluctuation of electric charge is larger at higher temperature. Note that RHIC has explored the temperature range $T > 0.2$ GeV for the first time ever. This tendency of dielectron production from the transport peak may be consistent with the dielectron production at SPS, which can be explained without the transport peak.

We list several future implications of interest: (i) First-principle calculation of transport coefficients and spectral function by lattice QCD is highly desirable. Calculation of the spectral function with finite momentum may give a clue to understanding the origin of low-mass dielectron enhancement. Some recent developments in such a direction can be seen in Refs. [39–42]. (ii) The event-by-event fluctuation of the initial geometry, which is expected to remain large at the early QGP phase, would enhance the dielectron production from the transport peak, as it does for real photon emission from high temperature region [43]. (iii) Since high-temperature QGP phase emits a large portion of thermal dileptons in spite of its small spacetime volume, the dielectron production from pre-equilibrium stage, or the so-called glasma, might also be important and thus needs to be evaluated.
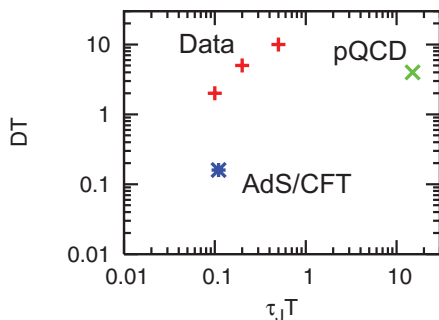
FIG. 8. (Color online) We plot parameter sets $(DT, \tau_J T)$ with which the experimental data dM/dm_{ee} are consistent. We also plot two limiting sets obtained by weak-coupling (pQCD) and strong-coupling (AdS/CFT) calculations.

APPENDIX A: MODEL OF LOW-MASS DILEPTONS: VECTOR MESON DOMINANCE

Here we assume vector meson dominance on the hadronic coupling to virtual photon and study its consequence on the dilepton spectra. Two standard scenarios, the dropping mass and the width broadening of the vector meson spectral function (VMD-SPF) will be considered.

1. Vector meson at finite temperature

We define the dimensionless spectral function at finite T as $\Sigma(q; T) \equiv -\mathrm{Im} G_{\mathrm{R},\mu}^{\mu}(q; T)/3q^2$. In the vacuum at $T = 0$, it can be is measured by the cross section of the electron-positron annihilation ($e^+e^- \to$ hadrons) and can be decomposed as

$$\Sigma(q; T = 0) = \sigma_\rho(q; T = 0) + \frac{1}{9}\sigma_\omega(q; T = 0) + \frac{1}{9}\sigma_\phi(q; T = 0), \quad (A1)$$

where $\sigma_\rho(q; T)$, $\sigma_\omega(q; T)$, $\sigma_\phi(q; T)$, and $\Sigma(q; T)$ correspond to the current correlations of $J_\rho^\mu = \frac{1}{2}(\bar{\mathrm{u}}\gamma^\mu \mathrm{u} - \bar{\mathrm{d}}\gamma^\mu \mathrm{d})$, $J_\omega^\mu = \frac{1}{2}(\bar{\mathrm{u}}\gamma^\mu \mathrm{u} + \bar{\mathrm{d}}\gamma^\mu \mathrm{d})$, $J_\phi^\mu = \bar{\mathrm{s}}\gamma^\mu \mathrm{s}$, and $J^\mu = J_\rho^\mu + \frac{1}{3}J_\omega^\mu - \frac{1}{3}J_\phi^\mu$, respectively.

The spectral function at zero temperature, $\Sigma(q; T = 0)$, has hadronic contribution at low q and perturbative QCD continuum at high q with an approximate continuum threshold at 1–1.5 GeV and may be parametrized as [44]

$$\sigma_V(q; T = 0) = \begin{cases} \frac{f_V^2 \Gamma_V m_V}{(q^2 - m_V^2)^2 + \Gamma_V^2 m_V^2} & (s_{0V} < q^2 < s_{1V}) \\ c_V & (s_{1V} < q^2) \end{cases}, \quad (A2)$$

with $V = \rho, \omega, \phi$. Here s_{0V} corresponds to the threshold associated with the decay into two pions (280 MeV) or three pions (420 MeV), while s_{1V} corresponds to the continuum threshold. We take the height of the continuum c_V from the leading-order perturbation theory and fit the other parameters (the resonance mass m_V, the resonance width Γ_V, the resonance height f_V, and the continuum threshold s_{1V}) by using experimental data in [45]. These parameters are listed in the Table I.

Since the ρ channel is a dominant source of the thermal component of the low-mass dileptons and is expected to receive the medium effect most strongly, we hereafter restrict our analysis on the medium modifications of $\sigma_\rho(q; T)$ at finite T within the same parametrization as Eq. (A2). Then the

TABLE I. The parameters of the vacuum spectral functions given in the unit of GeV except for dimensionless parameters c_v. They are obtained by fitting the experimental data [45].

Vector meson	m_V	Γ_V	f_V	$\sqrt{s_{0V}}$	$\sqrt{s_{1V}}$	c_V
ρ	0.77	0.15	0.15	0.28	1.3	$1/8\pi$
ω	0.78	0.008	0.14	0.42	1.1	$1/8\pi$
ϕ	1.02	0.004	0.24	0.42	1.5	$1/4\pi$

simplified form of the dilepton production rate reads

$$\frac{E_1 E_2 dN}{d^3 p_1 d^3 p_2 d^4 x}$$
$$= -\frac{\alpha^2}{6\pi^4 q^2}\left[\left(1 + \frac{2m_l^2}{q^2}\right)\mathrm{Im} G_{\mathrm{R},\mu}^{\mu}(q; T)\right]f_{\mathrm{BE}}(q^0; T)$$
$$\simeq \frac{\alpha^2}{2\pi^4}\left[\left(1 + \frac{2m_l^2}{q^2}\right)\sigma_\rho(q; T)\right]f_{\mathrm{BE}}(q^0; T), \quad (A3)$$

where we implicitly assume that the transverse and longitudinal spectral functions are the same even at finite T.

Let us now consider so-called dropping mass scenario where the mass parameters, $m_\rho(T)$ and $s_{1_\rho}(T)$, are assumed to scale with the chiral condensate [46–49]:

$$\frac{m_\rho(T)}{m_\rho(0)} = \frac{s_{1_\rho}(T)}{s_{1_\rho}(0)} = \frac{\langle\bar{q}q\rangle_T}{\langle\bar{q}q\rangle_0}. \quad (A4)$$

The scaling function in Eq. (A4) is obtained by fitting the latest lattice data (Fig. 4 (right) in Ref. [38]) by the following ansatz with $(T_c^*, \Delta) = (0.155\,\mathrm{GeV}, 0.025\,\mathrm{GeV})$:

$$\frac{\langle\bar{q}q\rangle_T}{\langle\bar{q}q\rangle_0} = \frac{1}{2}\left[1 - \tanh\left(\frac{T - T_c^*}{\Delta}\right)\right]. \quad (A5)$$

We assume that the pion mass does not change appreciably below T_c^* and adopt the following prescription for the low-energy threshold: $s_{0_\rho} = \min \cdot \{2m_\pi, \ m_\rho(T)\}$. Instead of introducing a parametrization for the T dependence of $\Gamma_\rho(T)$, we vary its value in the range 0.15–0.45 GeV to see its effect on the dilepton yield. Once it is given, remaining parameter, $f_\rho(T)$, is constrained by the QCD spectral sum rule [50]:

$$\int_0^\infty d\omega^2[\sigma_\rho(\omega, \vec{0}; T) - c_\rho] = 0. \quad (A6)$$

Shown in Fig. 9 is a resultant spectral function in the ρ channel with a parameter set, $(T_c^*, \Delta, \Gamma_\rho) = (0.155\,\mathrm{GeV}, 0.025\,\mathrm{GeV}, 0.3\,\mathrm{GeV})$.
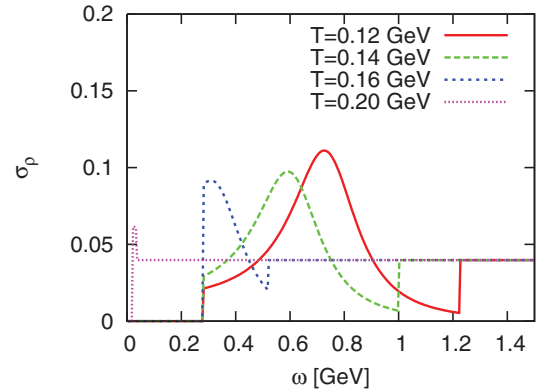

FIG. 9. (Color online) Shown is the scaled spectral function $\sigma_\rho(\omega, \vec{0}; T)$ as a function of ω at several different temperatures. The parameters in the spectral function are $(T_c^*, \Delta, \Gamma_\rho) = (0.155\,\mathrm{GeV}, 0.025\,\mathrm{GeV}, 0.3\,\mathrm{GeV})$.
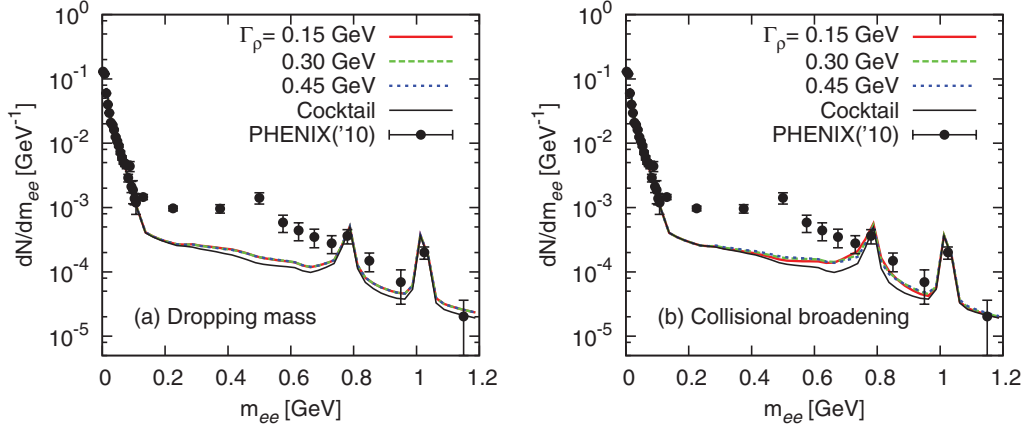
FIG. 10. (Color online) Shown in panels (a) and (b) are sum of the dielectron spectra from the thermal medium and the contributions from the hadronic decays after freezeout. The latter is denoted as "Cocktail" in these figures. The parameters of the VMD-SPF are $\Gamma_\rho = 0.15, 0.3, 0.45$ GeV and (a) $m_\rho(T) \propto \langle\bar{q}q\rangle_T$ (dropping mass) and (b) $m_\rho(T) = 0.77$ GeV (collisional broadening). These spectra are compared with experimental data of dielectron spectrum with minimum bias [7]. In panels (a) and (b), we plot only the statistical errors for experimental data.

2. Dielectron spectra

In Fig. 10, we compare the theoretical spectrum with the experimental data by taking into account the contributions from hadronic decays after freezeout (hadronic cocktail) given in Ref. [7]. The PHENIX acceptance is already taken into account. We show in Fig. 10(a) the thermal dielectron spectrum for $\Gamma_\rho = 0.15, 0.3, 0.45$ GeV and $m_\rho(T) = 0.77$ GeV (collisional broadening). It is clear from this figure that the dielectron emission with collisional broadening cannot explain only the experimental data in the low invariant mass region $m_{ee} < 0.6$ GeV. We show in Fig. 10(b) the thermal dielectron spectrum for $\Gamma_\rho = 0.15, 0.3, 0.45$ GeV and $m_\rho(T) \propto \langle\bar{q}q\rangle_T$. Even with the dropping mass, the dilepton yield undershoots the experimental data substantially in the low-invariant-mass region $m_{ee} < 0.6$ GeV. The above findings are consistent with the previous attempts to reproduce the low-mass dileptons at PHENIX [9–14].

APPENDIX B: EXTENSION OF TRANSPORT SPECTRAL FUNCTION TO MULTIFLAVOR CASE

We derive the transport spectral function for the multiflavor case. In this derivation, it is more convenient to treat flavor current for each quark species N_f^μ. We start from conservation laws in external field δA^μ, which couples to each flavor current and gives the perturbed Hamiltonian $\delta H(t) = \int d^3x \sum_f q_f N^\mu(x)\delta A_\mu(x)$:

$$\partial_\nu T^{\nu\mu} = F^{\mu\nu}\sum_f q_f N_{f,\nu}, \qquad (B1)$$

$$\partial_\mu N_f^\mu = 0 \quad (f = \mathrm{u, d, s}), \qquad (B2)$$

with $F_{\mu\nu} \equiv \partial_\mu \delta A_\nu - \partial_\nu \delta A_\mu$ and $q_\mathrm{u} = 2/3$, $q_\mathrm{d,s} = -1/3$. According to relativistic viscous hydrodynamics in the Landau

frame [34], we decompose $T^{\mu\nu}$ and N_f^μ as

$$T^{\mu\nu} = eu^\mu u^\nu - (P + \Pi)\triangle^{\mu\nu} + \pi^{\mu\nu}, \qquad (B3)$$

$$N_f^\mu = n_f u^\mu + \nu_f^\mu, \qquad (B4)$$

$$\triangle^{\mu\nu} \equiv g^{\mu\nu} - u^\mu u^\nu, \qquad (B5)$$

with bulk pressure Π, shear stress tensor $\pi^{\mu\nu}$, and dissipative flavor current ν_f^μ satisfying $\pi^{\mu\nu}u_\nu = 0$, $\pi_\mu^\mu = 0$, $\nu_f^\mu u_\mu = 0$. The entropy current in the second-order formalism [24,35,36] is decomposed as

$$\begin{aligned}
s^\mu = su^\mu &- \sum_f \frac{\mu_f}{T}\nu_f^\mu \\
&- \frac{u^\mu}{2T}\left(\beta_0\Pi^2 - \sum_{f,f'}\beta_1^{ff'}\nu_f^\mu\nu_{f',\mu} + \beta_2\pi^{\rho\sigma}\pi_{\rho\sigma}\right) \\
&- \frac{1}{T}\left(\sum_f \alpha_0^f \Pi \nu_f^\mu + \sum_f \alpha_1^f \pi^{\mu\nu}\nu_{f,\nu}\right), \qquad (B6)
\end{aligned}$$

with coupling coefficients α_0^f, α_1^f and $\beta_{0,2}$ ($\geqslant 0$), a positive semidefinite matrix $\beta_1^{ff'}$, and a chemical potential μ_f for each flavor. Divergence of the entropy current by using Eqs. (B3) and (B4) up to second-order deviation from equilibrium is

$$\begin{aligned}
\partial_\mu s^\mu = &-\frac{\Pi}{T}\left(\triangle^{\mu\nu}\partial_\mu u_\nu + \beta_0\dot{\Pi} + \sum_f \alpha_0^f \partial_\mu \nu_f^\mu\right) \\
&+ \frac{\pi^{\mu\nu}}{T}\left(\partial_\mu u_\nu - \beta_2\dot{\pi}_{\mu\nu} - \sum_f \alpha_1^f \partial_\mu \nu_{f,\nu}\right) \\
&- \sum_f \frac{\nu_f^\mu}{T}\left[T\partial_\mu\left(\frac{\mu_f}{T}\right) + q_f F_{\mu\nu}u^\nu\right. \\
&\left. - \sum_{f'} \beta_1^{ff'}\dot{\nu}_{f',\mu} + \alpha_0^f \partial_\mu \Pi + \alpha_1^f \partial_\nu \pi_\mu^\nu\right], \quad (B7)
\end{aligned}$$

where $\dot{f} \equiv u^\mu \partial_\mu f$. Constitutive equations which ensure the second law of thermodynamics are obtained as follows:

$$-\Pi = \zeta \left(\triangle^{\mu\nu} \partial_\mu u_\nu + \beta_0 \dot{\Pi} + \sum_f \alpha_0^f \partial_\mu \nu_f^\mu \right), \quad (B8)$$

$$\pi^{\mu\nu} = 2\eta \left\langle\!\!\left\langle \partial^\mu u^\nu - \beta_2 \dot{\pi}^{\mu\nu} - \sum_f \alpha_1^f \partial^\mu \nu_f^\nu \right\rangle\!\!\right\rangle, \quad (B9)$$

$$\nu_f^\mu = \sigma_f \triangle_\rho^\mu \sum_{f'} \kappa^{ff'} \left[T\partial^\rho \left(\frac{\mu_{f'}}{T} \right) + q_{f'} F_\sigma^\rho u^\sigma \right.$$
$$\left. - \sum_{f''} \beta_1^{f'f''} \dot{\nu}_{f''}^\rho + \alpha_0^{f'} \partial^\rho \Pi + \alpha_1^{f'} \partial_\sigma \pi^{\sigma\rho} \right], \quad (B10)$$

with bulk and shear viscosities ζ, η (≥ 0), flavor conductivity σ_f (≥ 0), and a positive semidefinite flavor mixing matrix $\kappa^{ff'}$. $\langle\!\langle B^{\mu\nu} \rangle\!\rangle$ stands for

$$\langle\!\langle B^{\mu\nu} \rangle\!\rangle \equiv \triangle^{\mu\rho} \triangle^{\nu\sigma} \left[\frac{B_{\rho\sigma} + B_{\sigma\rho}}{2} - \frac{\triangle_{\rho\sigma} \triangle^{\alpha\beta} B_{\alpha\beta}}{3} \right]. \quad (B11)$$

We perform linear analysis in terms of δe, δn_f, and $\delta \vec{u}$ defined as

$$e(x) = e + \delta e(x), \quad (B12)$$

$$n_f(x) = n_f + \delta n_f(x), \quad (B13)$$

$$u^\mu(x) = (1, \; \delta\vec{u}(x)), \quad (B14)$$

and external vector field δA^μ. For simplicity we neglect the couplings between different dissipative terms: $\alpha_0^f = \alpha_1^f = 0$, $\beta_1^{ff'} = \beta^f \delta_{ff'}$, and $\kappa^{ff'} = \kappa^f \delta_{ff'}$ [assumption (i)]. The dissipative flavor current $\nu_f^\mu(x)$ is then given by

$$\nu_f^0(x) = 0, \quad (B15)$$

$$\vec{\nu}_f(x) = -\sigma_f \left[T\vec{\nabla} \left(\frac{\mu_f}{T} \right) - q_f \vec{E} + \beta_1^f \partial_t \vec{\nu}_f \right], \quad (B16)$$

in the linear order in δe, δn_f, $\delta \vec{u}$, and A^μ. We define susceptibility matrices X and X_{f} as

$$X \equiv \begin{pmatrix} \frac{\partial e}{\partial T} & \frac{\partial e}{\partial \mu_u} & \frac{\partial e}{\partial \mu_d} & \frac{\partial e}{\partial \mu_s} \\ \frac{\partial n_u}{\partial T} & \frac{\partial n_u}{\partial \mu_u} & \frac{\partial n_u}{\partial \mu_d} & \frac{\partial n_u}{\partial \mu_s} \\ \frac{\partial n_d}{\partial T} & \frac{\partial n_d}{\partial \mu_u} & \frac{\partial n_d}{\partial \mu_d} & \frac{\partial n_d}{\partial \mu_s} \\ \frac{\partial n_s}{\partial T} & \frac{\partial n_s}{\partial \mu_u} & \frac{\partial n_s}{\partial \mu_d} & \frac{\partial n_s}{\partial \mu_s} \end{pmatrix},$$

$$X_{\mathrm{f}} \equiv \begin{pmatrix} \frac{\partial n_u}{\partial \mu_u} & \frac{\partial n_u}{\partial \mu_d} & \frac{\partial n_u}{\partial \mu_s} \\ \frac{\partial n_d}{\partial \mu_u} & \frac{\partial n_d}{\partial \mu_d} & \frac{\partial n_d}{\partial \mu_s} \\ \frac{\partial n_s}{\partial \mu_u} & \frac{\partial n_s}{\partial \mu_d} & \frac{\partial n_s}{\partial \mu_s} \end{pmatrix}. \quad (B17)$$

Then the dissipative flavor current ν_f^μ is obtained as

$$\nu_f^0 = 0,$$

$$\vec{\nu}_f = q_f \sigma_f \vec{E} - \beta_{f,1} \sigma_f \partial_t \vec{\nu}_f - \sigma_f \left(-\frac{\mu_f}{T}, \{\vec{e}_f\} \right) X^{-1} \begin{pmatrix} \vec{\nabla} \delta e \\ \vec{\nabla} \delta n_u \\ \vec{\nabla} \delta n_d \\ \vec{\nabla} \delta n_s \end{pmatrix}, \quad (B18)$$

$$\{\vec{e}_u\} \equiv \{1, 0, 0\}, \quad \{\vec{e}_d\} \equiv \{0, 1, 0\}, \quad \{\vec{e}_s\} \equiv \{0, 0, 1\}. \quad (B19)$$

We make another simplification that σ_f and β_1^f are flavor independent [assumption (ii)]:

$$\sigma_f \equiv \bar{\sigma}, \quad \beta_1^f \equiv \bar{\beta}_1, \quad (B20)$$

and restrict ourselves to the situation with vanishing flavor chemical potential $\mu_f = 0$, which decouples flavor dissipation and sound mode propagation. We then arrive at

$$\vec{\nu}_f + \bar{\beta}_1 \bar{\sigma} \frac{\partial}{\partial t} \vec{\nu}_f = q_f \bar{\sigma} \vec{E} - \bar{\sigma} \{\vec{e}_f\} X_{\mathrm{f}}^{-1} \begin{pmatrix} \vec{\nabla} \delta n_u \\ \vec{\nabla} \delta n_d \\ \vec{\nabla} \delta n_s \end{pmatrix}. \quad (B21)$$

So far we have simplified transport coefficients in order to reduce unknown parameters and to avoid mode couplings. In order to obtain simple constitutive equation for diffusive electric current in the multiflavor case, it is necessary to simplify thermodynamic quantities, namely susceptibility matrix to be $X_{\mathrm{f}} \approx (\partial n_u/\partial \mu_u)\mathbf{1} \equiv \chi_{uu}\mathbf{1}$ [assumption (iii)]. This yields

$$\vec{\nu}_f + \bar{\beta}_1 \bar{\sigma} \frac{\partial}{\partial t} \vec{\nu}_f = q_f \bar{\sigma} \vec{E} - \frac{\bar{\sigma}}{\chi_{uu}} \vec{\nabla} \delta n_f. \quad (B22)$$

Note that by this simplification we also obtain electric charge susceptibility χ in terms of u-quark number susceptibility $\chi = (2/3)\chi_{uu}$. Then constitutive equation for diffusive electric current is given by

$$\delta n \equiv \sum_f q_f \delta n_f, \quad \vec{\nu} \equiv \sum_f q_f \vec{\nu}_f,$$
$$\vec{\nu} + \bar{\beta}_1 \bar{\sigma} \frac{\partial}{\partial t} \vec{\nu} = \frac{2}{3} \bar{\sigma} \vec{E} - \frac{2\bar{\sigma}}{3\chi} \vec{\nabla} \delta n. \quad (B23)$$

In comparison with Eq. (31), transport coefficients for the electric current are related to those for flavor currents by

$$\tau_{\mathrm{J}} = \bar{\beta}_1 \bar{\sigma}, \quad \sigma = \frac{2}{3} \bar{\sigma}, \quad D = \frac{2\bar{\sigma}}{3\chi}, \quad (B24)$$

satisfying $\sigma = \chi D$.

We are also interested in the constitutive equation for diffusive quark number current. Then we need to modify Eq. (B23) by substituting $q_f \rightarrow 1$, $\delta A^\mu \rightarrow \delta A_{\mathrm{q}}^\mu$, and $\vec{E} \rightarrow \vec{E}_{\mathrm{q}}$, where $\delta A_{\mathrm{q}}^\mu$ denotes an external vector field that couples with quark number current. Note also that total quark number susceptibility is $\chi_{\mathrm{q}} = 3\chi_{uu}$ because of the simplification for X_{f}. Then we get

$$\delta n_{\mathrm{q}} \equiv \sum_f \delta n_f, \quad \vec{\nu}_{\mathrm{q}} \equiv \sum_f \vec{\nu}_f,$$
$$\vec{\nu}_{\mathrm{q}} + \bar{\beta}_1 \bar{\sigma} \frac{\partial}{\partial t} \vec{\nu}_{\mathrm{q}} = 3\bar{\sigma} \vec{E}_{\mathrm{q}} - \frac{3\bar{\sigma}}{\chi_{\mathrm{q}}} \vec{\nabla} \delta n_{\mathrm{q}}, \quad (B25)$$

$$\tau_{\mathrm{q}} = \bar{\beta}_1 \bar{\sigma}, \quad \sigma_{\mathrm{q}} = 3\bar{\sigma}, \quad D_{\mathrm{q}} = \frac{3\bar{\sigma}}{\chi_{\mathrm{q}}}, \quad (B26)$$

satisfying $\sigma_{\mathrm{q}} = \chi_{\mathrm{q}} D_{\mathrm{q}}$. Therefore we can verify $D = D_{\mathrm{q}}$, which we use in the text.

[1] P. F. Kolb and U. W. Heinz, in *Quark Gluon Plasma 3*, edited by R. C. Hwa and X.-N. Wang (World Scientific, Singapore, 2004), pp. 634–714.

[2] P. Huovinen and P. V. Ruuskanen, Ann. Rev. Nucl. Part. Sci. **56**, 163 (2006).

[3] T. Hirano, N. van der Kolk, and A. Bilandzic, Lect. Notes Phys. **785**, 139 (2010).

[4] M. Gyulassy, I. Vitev, X.-N. Wang, and B.-W. Zhang, in *Quark Gluon Plasma 3*, edited by R. C. Hwa and X.-N. Wang (World Scientific, Singapore, 2004), pp. 123–191.

[5] W. A. Horowitz, Nucl. Phys. A **855**, 225 (2011).

[6] PHENIX Collaboration, S. Afanasiev *et al.*, arXiv:0706.3034 [nucl-ex].

[7] A. Adare *et al.* (PHENIX Collaboration), Phys. Rev. C **81**, 034911 (2010).

[8] J. Zhao *et al.* (STAR Collaboration), J. Phys. G **38**, 124134 (2011).

[9] R. Rapp, AIP Conf. Proc. **1322**, 55 (2010).

[10] S. Ghosh, S. Sarkar, and J. E. Alam, Eur. Phys. J. C **71**, 1760 (2011).

[11] K. Dusling and I. Zahed, Nucl. Phys. A **825**, 212 (2009).

[12] K. Dusling and I. Zahed, Phys. Rev. C **82**, 054909 (2010).

[13] E. L. Bratkovskaya, W. Cassing, and O. Linnyk, Phys. Lett. B **670**, 428 (2009).

[14] E. L. Bratkovskaya, O. Linnyk, and W. Cassing, J. Phys.: Conf. Ser. **230**, 012032 (2010).

[15] P. Aurenche, F. Gelis, G. D. Moore, and H. Zaraket, J. High Energy Phys. 12 (2002) 006.

[16] S. Jeon, Phys. Rev. D **52**, 3591 (1995).

[17] P. B. Arnold, G. D. Moore, and L. G. Yaffe, J. High Energy Phys. 11 (2000) 001.

[18] P. B. Arnold, G. D. Moore, and L. G. Yaffe, J. High Energy Phys. 05 (2003) 051.

[19] J. Hong and D. Teaney, Phys. Rev. C **82**, 044908 (2010).

[20] Y. Hidaka and T. Kunihiro, Phys. Rev. D **83**, 076004 (2011).

[21] G. Aarts and J. M. Martinez Resco, J. High Energy Phys. 04 (2002) 053.

[22] J. I. Kapusta and C. Gale, *Finite-Temperature Field Theory* (Cambridge University Press, Cambridge, 2006).

[23] L. P. Kadanoff and P. C. Martin, Ann. Phys. **24**, 419 (1963).

[24] M. Natsuume and T. Okamura, Phys. Rev. D **77**, 066014 (2008); **78**, 089902 (2008).

[25] S. Borsanyi *et al.*, J. High Energy Phys. 11 (**2010**) 077.

[26] M. L. Miller, K. Reygers, S. J. Sanders, and P. Steinberg, Ann. Rev. Nucl. Part. Sci. **57**, 205 (2007).

[27] T. Hirano, Phys. Rev. C **65**, 011901 (2001).

[28] T. Hirano and K. Tsuda, Phys. Rev. C **66**, 054905 (2002).

[29] T. Hirano, U. W. Heinz, D. Kharzeev, R. Lacey, and Y. Nara, Phys. Lett. B **636**, 299 (2006).

[30] T. Hirano, U. W. Heinz, D. Kharzeev, R. Lacey, and Y. Nara, Phys. Rev. C **77**, 044909 (2008).

[31] F. Cooper and G. Frye, Phys. Rev. D **10**, 186 (1974).

[32] E. L. Feinberg, Nuovo Cimento A **34**, 391 (1976).

[33] L. D. McLerran and T. Toimela, Phys. Rev. D **31**, 545 (1985).

[34] L. D. Landau and E. M. Lifshitz, *Fluid Mechanics* (Pergamon Press, Oxford, 1987).

[35] W. Israel, Ann. Phys. **100**, 310 (1976).

[36] W. Israel and J. M. Stewart, Ann. Phys. **118**, 341 (1979).

[37] C. R. Allton *et al.*, Phys. Rev. D **71**, 054508 (2005).

[38] Wuppertal-Budapest Collaboration, S. Borsanyi, Z. Fodor, C. Hoelbling, S. D. Katz, S. Krieg, C. Ratti, and K. K. Szabo, J. High Energy Phys. 09 (2010) 073.

[39] G. Aarts, C. Allton, J. Foley, S. Hands, and S. Kim, Phys. Rev. Lett. **99**, 022002 (2007).

[40] G. Aarts, C. R. Allton, S. J. Hands, J. Foley, and S. Kim, PoS Lattice **2010**, 166 (2010).

[41] H. T. Ding, A. Francis, O. Kaczmarek, F. Karsch, E. Laermann, and W. Soeldner, Phys. Rev. D **83**, 034504 (2011).

[42] H.-T. Ding, A. Francis, O. Kaczmarek, F. Karsch, H. Satz, and W. Söeldner, J. Phys. G **38**, 124070 (2011).

[43] R. Chatterjee, H. Holopainen, T. Renk, and K. J. Eskola, Phys. Rev. C **83**, 054908, (2011).

[44] E. V. Shuryak, Rev. Mod. Phys. **65**, 1 (1993).

[45] K. Nakamura *et al.* (Particle Data Group), J. Phys. G **37**, 075021 (2010).

[46] R. D. Pisarski, Phys. Lett. B **110**, 155 (1982).

[47] G. E. Brown and M. Rho, Phys. Rev. Lett. **66**, 2720 (1991).

[48] T. Hatsuda and S. H. Lee, Phys. Rev. C **46**, 34 (1992).

[49] E. Marco and W. Weise, Phys. Lett. B **482**, 87 (2000).

[50] T. Hatsuda, Y. Koike, and S. H. Lee, Nucl. Phys. B **394**, 221 (1993).